Article

Discovery Medicine 2025; 37(203): 2990–3002
https://doi.org/10.24976/Discov.Med.202537203.250

Ursolic Acid Ameliorates Osteoporosis via Gut Microbiota Remodeling and Enrichment of Probiotic Species

Morong Wu[1,†], Zhengsheng Bao[1,†], Jingyuan Wen[2], Longkang Cui[3], Gaobo Shen[3], Xuefeng Li[2], Bingbing Zhang[3], Lixia Jin[4,*], Yang Yu[1,*]

[1]The Second Clinical College, Zhejiang Chinese Medical University, 310000 Hangzhou, Zhejiang, China
[2]The First Clinical College, Zhejiang Chinese Medical University, 310000 Hangzhou, Zhejiang, China
[3]Department of Orthopedic Surgery, The Second Affiliated Hospital of Zhejiang Chinese Medical University, 310000 Hangzhou, Zhejiang, China
[4]School of Medical Technology and Information Engineering, Zhejiang Chinese Medical University, 310000 Hangzhou, Zhejiang, China
*Correspondence: windyjinlx@zcmu.edu.cn (Lixia Jin); 202311020811068@zcmu.edu.cn (Yang Yu)
[†]These authors contributed equally.
Submitted: 27 August 2025 Revised: 22 October 2025 Accepted: 30 October 2025 Published: 20 December 2025

Background: The association between osteoporosis (OP) and gut microbiota (GM) has been extensively investigated to identify novel probiotics for disease management for effective OP treatment remains imperative. Ursolic acid (UA), a natural triterpenoid compound, has been shown to reduce bone loss caused by ovariectomy (OVX); however, the contribution of GM in this reduction remains unclear. Therefore, this study investigates the impact of UA on OP and demonstrates that it ameliorates disease by remodeling the GM, with metagenomic sequencing identifying potential probiotics that likely mediate these effects.

Methods: OVX mice received daily UA (200 mg/kg) or vehicle for 7 weeks. Bone mass and microarchitecture were assessed via microcomputed tomography (micro-CT) and Alisin Blue Haematoxylin/Orange G (ABH) staining. Bone formation (Runx2, alkaline phosphatase (ALP), osteocalcin (OCN) immunohistochemistry) and resorption (tartrate-resistant acid phosphatase (TRAP) staining) were evaluated in these treated mice. Fecal microbiota transplantation (FMT) from UA-treated donors to antibiotic-pre-treated OVX recipients was performed to test GM causality. The gut microbial composition was analyzed using metagenomic sequencing, with key species identified via Linear Discriminant Analysis Effect Size (LEfSe) and correlated with bone parameters. To further investigate the impact of *Parabacteroides goldsteinii* (*P. goldsteinii*) on bone mass, OVX mice were administered either live *P. goldsteinii*, pasteurized *P. goldsteinii* or PBS via oral gavage daily for 6 weeks. Micro-CT analysis was used to evaluate the effect of *P. goldsteinii* on bone mass.

Results: UA treatment significantly increased bone mineral density (BMD, $p < 0.01$), bone volume fraction (BV/TV, $p < 0.05$), and trabecular thickness (Tb.Th, $p < 0.001$), while decreasing trabecular separation (Tb.Sp, $p < 0.01$) in OVX mice. Critically, FMT from UA-treated donors recapitulated these osteoprotective effects in recipient OVX mice, confirming the mediating role of GM. Metagenomic analysis revealed that UA significantly altered GM structure, enriching *Akkermansia muciniphila* (*A. muciniphila*, $p < 0.01$) and *P. goldsteinii* ($p < 0.01$). Abundance of *A. muciniphila* strongly correlated with improved BV/TV ($p < 0.01$), and Tb.Th ($p < 0.05$), and reduced Tb.Sp ($p < 0.01$). *P. goldsteinii* abundance also showed a significant positive correlation with BMD ($p < 0.05$) and a negative correlation with Tb.Sp ($p < 0.01$). Furthermore, *P. goldsteinii* significantly increased the BMD of the distal femur ($p < 0.05$), BV/TV ($p < 0.05$), and Tb.Th ($p < 0.01$), while decreasing Tb.Sp ($p < 0.001$) in OVX mice.

Conclusion: GM contributes to the protective effect of UA against osteoporosis, mediated by the enrichment of specific probiotics such as *A. muciniphila* and *P. goldsteinii*. This study provides the first direct evidence that *P. goldsteinii* supplementation protects against bone loss, making it a promising probiotic candidate for managing OP.

Keywords: osteoporosis; ursolic acid; gut microbiota; *Akkermansia muciniphila*; *Parabacteroides goldsteinii*

Introduction

Osteoporosis (OP) is a common metabolic bone disease among elderly individuals, characterized by reduced bone mass, compromised bone microstructure, and a high risk of osteoporotic fractures [1–3]. The incidence of OP continues to rise with population aging, and a recent study reported a global prevalence of approximately 21.7% among older adults [4]. Given its high prevalence and the substantial costs associated with management, OP imposes significant medical and economic burdens on patients and society. While studies on pathogenesis have focused on bone tissue, increasing evidence, in recent years, links the gut microbiota (GM) to the development and progression of

OP. Furthermore, the emerging gut-bone axis concept underscores the GM as a promising therapeutic target for OP [5].

The GM, often referred to as the "second human genome", constitutes the most complex microbial system, comprising approximately 10–100 trillion microorganisms. Its composition is highly individualized and is significantly influenced by host genotype, age, sex, dietary habits, physical activity, and environmental exposures. The GM influences the development of various diseases through several mechanisms, including effects on digestion, nutrient absorption, energy homeostasis, immune regulation, essential vitamin synthesis, and maintenance of the intestinal barrier [6,7]. Importantly, depletion of the microbiota has been shown to protect mice from bone loss induced by sex hormone deficiency [8], whereas transplanting gut microbiota from mice with normal bone mass restores bone mass in depleted recipients [9].

Furthermore, the intestinal microbiota can enhance bone mass through various mechanisms, including modulation of immune homeostasis [10], production of short-chain fatty acids [11], restoration of intestinal barrier integrity [12], and secretion of extracellular vesicles [13]. Collectively, these findings suggest that modulating the GM and identifying probiotics that improve bone metabolism represent promising therapeutic strategies for OP. However, the clinical translation of these probiotics remains hindered by challenges such as competitive exclusion by the host intestinal flora and inadequate acid and bile salt tolerance in some strains [14]. Identifying robust, novel probiotics candidates for effective OP treatment is therefore crucial.

Owing to the severe side effects and complications associated with several current osteoporosis drugs, long-term use is often discouraged. Consequently, there is a pressing demand for safer and more efficacious anti-osteoporotic agents. Ursolic acid (UA), a naturally occurring pentacyclic triterpenoid, is widely distributed in the plants, notably in the fruit peels (such as apple), common culinary herbs (e.g., rosemary, thyme, and oregano), and the leaves, flowers, bark, or epicuticular waxes of numerous plants, including lavender, eucalyptus, black elder, hawthorn, and coffee [15]. Evidence demonstrates that UA ameliorates bone loss and microstructural deterioration induced by ovariectomy (OVX) or retinoic acid in rats, enhancing osteoblast activity while inhibiting osteoclast activity [16,17]. Its osteoprotective effects may involve inhibiting autophagy-mediated osteoclast differentiation and activating signaling pathways such as mitogen-activated protein kinases (MAPKs), nuclear factor-kappa B (NF-κB), and activator protein-1 (AP-1) to induce osteoblast-specific gene expression [18]. Recent evidence further indicates that UA can ameliorate gut microbiota dysbiosis in various disease models [19].

However, whether the beneficial effects of UA on bone metabolism depend on the modulation of the gut microbiota remains unclear. Therefore, this study aimed to determine whether UA-induced improvements in bone metabolism are associated with alterations in the gut microbiota. We employed metagenomic sequencing to identify potential probiotics that could mediate therapeutic effects, thereby investigating the mechanism of UA in OP treatment from the perspective of gut microbiota regulation.

Methods

Experimental Animal Model

Eight-week-old female C57BL/6J mice were obtained from the Experimental Animal Research Center of Zhejiang University of Traditional Chinese Medicine and were housed individually under controlled conditions (24 $\pm$ 1 °C, 12/12-h light/dark) with free access to sterile chow and water. Following a 2-week acclimation period, all mice received an intramuscular atropine (0.04 mg/kg), followed by intraperitoneal anesthesia with zolertil (50 mg/kg) 15 min later. Mice were categorized as the Vehicle and UA groups and then underwent bilateral ovariectomy as previously described [20].

Briefly, a dorsal midline incision was made, the ovaries were exposed, ligated, and then resected bilaterally. Mice in the SHAM group underwent the same surgical procedure without ovary removal. To assess the therapeutic effect of UA, mice in the UA group received daily oral gavage of 200 mg/kg UA (#U6753, Sigma-Aldrich) in corn oil initiated one week after surgery. The SHAM and Vehicle groups received an equivalent volume of corn oil via oral gavage. Treatment continued for 7 weeks, and mice were euthanized by intraperitoneal injection of pentobarbital sodium (150 mg/kg). Bilateral distal femurs were scanned using micro-CT. For subsequent bone histology and immunohistochemical staining, femurs were fixed in 4% paraformaldehyde (PFA)(#J19943.K2, Thermo Fisher Scientific), then decalcified.

For the *Parabacteroides goldsteinii* (*P. goldsteinii*) efficiency assay in OVX mice, mice were divided into three groups. One treatment group was administered orally with live *P. goldsteinii* (LPG) at 2 $\times$ 10^8 cfu per mouse. The second treatment group received pasteurized *P. goldsteinii* (PPG; 2 $\times$ 10^8 cfu) suspended in 0.2 mL of sterile anaerobic PBS, administered daily by mouth. The vehicle group received an equivalent volume of sterile anaerobic PBS by gavage. These treatments continued for 6 weeks.

Fecal Microbiota Transplantation (FMT)

Fecal samples were collected from the UA and Vehicle groups of mice daily for 4 weeks before euthanasia and stored at –80 °C. Before fecal microbiota transplantation (FMT), the fecal samples were diluted in anaerobic PBS to 40 mg/mL, homogenized, and filtered through a 0.25-mm stainless steel sieve. Recipient mice received a broad-spectrum antibiotic cocktail in drinking water for one week, containing ampicillin (1 g/L)(#HY-

B0522, MCE), metronidazole (1 g/L)(#HY-B0318, MCE), neomycin (1 g/L)(#N1420253, Aladdin), and vancomycin (0.5 g/L)(#V421514, Aladdin). Following a 24-hwashout with regular water, each recipient mouse received 200 µL of donor fecal mixture by oral gavage three times per week for 6 weeks. Recipient mice in the antibiotic (Abx) group received sterile PBS via gavage.

Microcomputed Tomography (Micro-CT)

Distal femur samples were scanned using a microcomputed tomography (micro-CT) system (SkyScan1176; Bruker, Kontich, Belgium) at 45 kV, 500 µA, with an exposure time of 770 ms. Images were visualized and reconstructed in three dimensions with the SkyScan software (CTVolx v3.0, Bruker microCT, Kontich, Belgium). Trabecular parameters, including bone mineral density (BMD, mg/cm^3), trabecular bone volume fraction (BV/TV, %), trabecular thickness (Tb.Th, mm), and trabecular separation (Tb.Sp, mm), were quantified with CTAn software (v1.15, CTVolx v3.0, Bruker microCT, Kontich, Belgium).

Bone Tissue Morphometry and Immunohistochemistry

For bone morphometry and immunohistochemistry, distal femur samples were demineralized in 14% EDTA (pH 7.2)(#A500838-0500, Sangon Biotech) for 15 days following micro-CT scanning, then dehydrated using a gradient of alcohol. Samples were embedded in paraffin in a sagittal orientation and sectioned at 3-µm using a microtome (#HM355S, Thermo Fisher Scientific) for all histologic and immunohistochemical procedures.

Bone microstructure was assessed via Alisin Blue Haematoxylin/Orange G (ABH) staining. Briefly, sections were deparaffinized, washed three times in PBS, immersed in 1% hydrochloric acid alcohol for 30 s, and then stained with Alisin Blue dye for 1 h. The samples were immersed in 1% hydrochloric acid for 5 s, washed in purified water, neutralized in 0.5% ammonia for 15 s, washed again, immersed in 95% alcohol for 1 min, stained with Orange G dye for 90 s, washed, and dried at 37 °C. Changes in bone microstructure were then observed and photographed under light microscopy.

The number of osteoclasts along the trabecular surface was evaluated by tartrate-resistant acid phosphatase (TRAP) staining (Kit #387-1KT, Sigma-Aldrich). Briefly, tissue sections were rehydrated and incubated at 37 °C for 1 h in a basic stock solution containing naphthol AS-BI phosphate (0.2 mg/mL). Sections were then incubated at 37 °C for 10 min in a mixture of sodium nitrite (0.8 mg/mL) and pararosaniline (1.0 mg/mL), followed by hematoxylin counterstaining. Multinuclear TRAP-positive cells adjacent to the distal femoral growth plate were quantified using ImageJ software (version 1.5, National Institutes of Health, Bethesda, MD, USA). The quantitative analysis was performed according to the standard principles of bone histomorphometry. Specifically, only TRAP-positive cells that were located in direct contact with and firmly attached to the trabecular bone surface were identified and counted as mature osteoclasts. The raw osteoclast count was then normalized to the total length of the trabecular bone surface over which the counting was performed, yielding the parameter N.Oc/BS (Number of Osteoclasts per unit Bone Surface, units: #/mm).

Immunohistochemical staining was performed to evaluate the expression levels of Runx2, osteocalcin (OCN), and alkaline phosphatase (ALP) in bone tissue. Sections were deparaffinized in xylene (#534056,Sigma-Aldrich) (3 × 10 min) and rehydrated through a graded ethanol series (100%, 100%, 95%, 85%, 75%; 5 min each), then washed with distilled water. Antigen retrieval was achieved in 10 mM sodium citrate buffer (#C7254, Sigma-Aldrich) (pH 6.0) at 65 °C for 4 h. Endogenous peroxidase activity was blocked with 3% H_2O_2 (#H1009, Sigma-Aldrich) at 25 °C for 10 min, followed by three 3-min PBS washes. Non-specific binding was inhibited with 10% normal goat serum (#ZLI-9056, ZSGB-BIO) at 37 °C for 30 min. After three PBS washes, tissue sections were incubated with primary antibodies at 4 °C overnight.

The following day, tissue sections underwent three PBS washes, followed by incubation at 37 °C for 30 min with horseradish peroxidase-conjugated secondary antibodies (PV-9001, ZSGB-BIO, Beijing, China). Color development was achieved with DAB chromogen (Dako) (#K3468, Agilent Dako) under microscopic monitoring. Nuclei were counterstained with hematoxylin (#MHS32, Sigma-Aldrich) to enhance morphological visualization. Sections were then dehydrated through an ascending ethanol gradient (75%–100%), cleared in xylene (3 × 5 min), and mounted with neutral gum under cover slips. Slides were observed under a light microscope, and images were recorded.

Primary antibodies used in the present study were as follows: anti-ALP antibody (1:200, #ARG57422, Arigo), anti-OCN antibody (1:200, #A20800, ABclonal), and anti-Runx2 antibody (1:200, #ab236639, Abcam). Positively stained areas were quantified using ImageJ software (version 5.0, National Institutes of Health, Bethesda, MD, USA).

Macrogenome Sequencing

Genomic DNA was extracted from fecal samples using the Fecal Genome DNA Extraction Kit (AU46111-96, BioTeke). DNA libraries were prepared using the TruSeq Nano DNA Library Preparation Kit (Set #FC-121-4001), following the manufacturer's instructions. Metagenomic sequencing was conducted on an Illumina NovaSeq 6000 platform (PE150) at LC-Bio Technology Co., Ltd. (Hangzhou, China).

Raw reads were processed with Fastp (v0.23.4) to eliminate adapter sequences, low-quality bases (Q < 20),

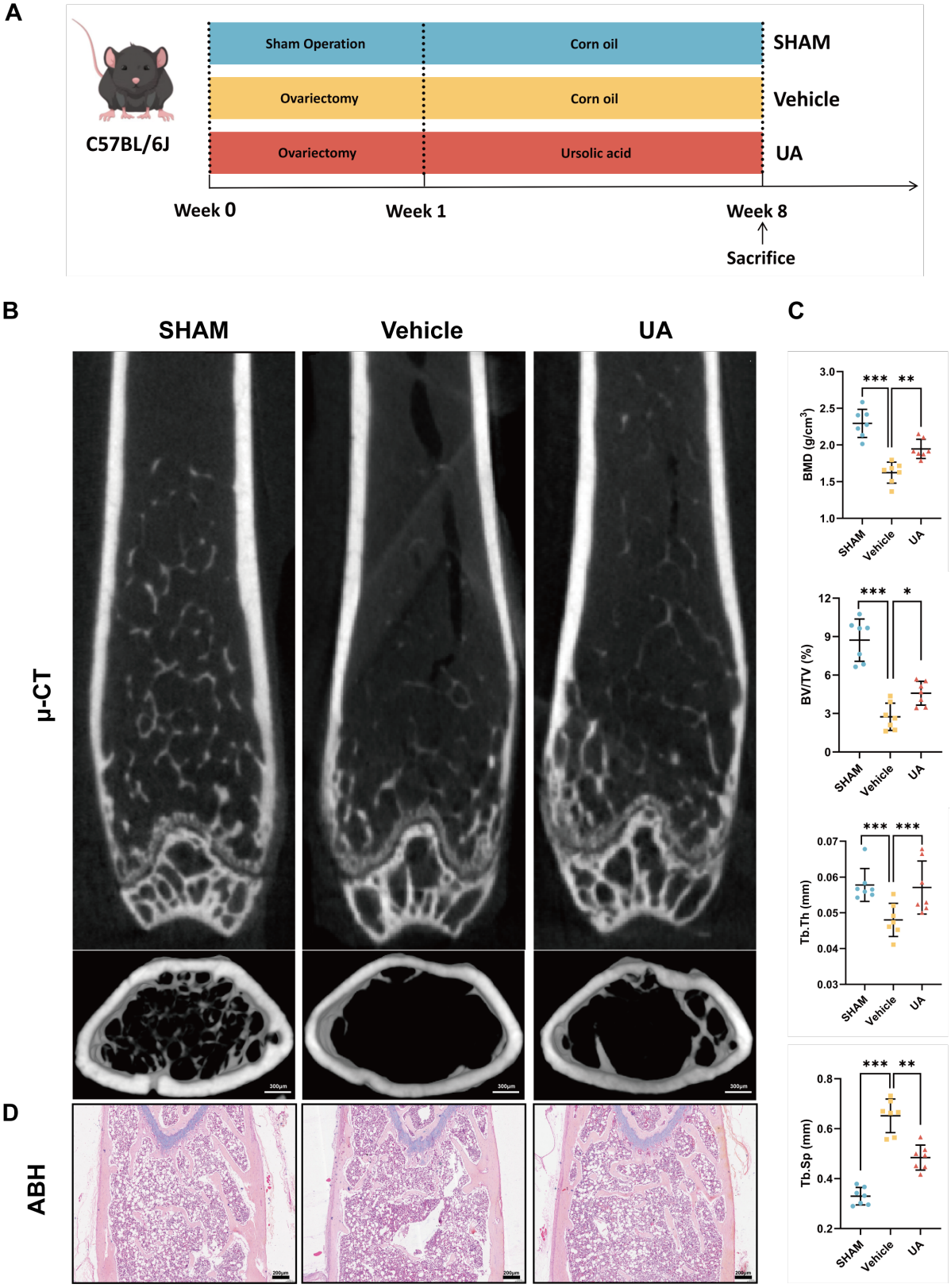

Fig. 1. UA alters bone mass and bone microarchitecture in OVX mice. (A) Experimental design timeline. The mice underwent sham or OVX surgery, followed by daily oral gavage of UA (200 mg/kg) or corn oil (vehicle) from postoperative week 1 to week 8. (B) Micro-CT results showing trabecular bone architecture in the distal femur. (C,D) Micro-CT scanning and ABH staining of the trabecular bone microarchitecture. The graphs present the means ± SDs (n = 7). ***$p < 0.001$, **$p < 0.01$, *$p < 0.05$. UA, ursolic acid; OVX, ovariectomy; micro-CT, microcomputed tomography; ABH, Alisin Blue Haematoxylin/Orange G.

and ambiguous bases. Host DNA contamination was filtered by aligning quality-control reads to the mouse reference genome (Mus_musculus, Ensembl release 101) using Bowtie2 (v2.2). *De novo* assembly of the remaining reads was performed per sample with MEGAHIT (v1.2.9) and resulting contigs were used for microbial taxonomic and functional analyses. Coding sequences (CDSs) were predicted with MetaGeneMark (v3.26) and clustered across all samples into unigenes using MMseq2 (v15-6f452). Taxonomic assignment of the microbiota was performed by aligning protein sequences to the NCBI nonredundant (NR) database with DIAMOND (v0.9.14). Species-level differential abundance was assessed using the Wilcoxon rank-sum test, with statistical significance set at $p < 0.05$ and a |log2-fold change| threshold >1. Alpha diversity indices, including the Chao1 index (estimating richness), Shannon index (estimating evenness and richness), and the number of observed species, were calculated from the species abundance profile of each sample using QIIME2 (version 2023.5). The statistical differences in these alpha diversity indices between the UA-treated and Vehicle-treated groups were assessed using the Wilcoxon rank-sum test in R software (version 4.2.1, R Foundation for Statistical Computing, Vienna, Austria). A *p*-value of less than 0.05 was considered statistically significant. For beta diversity analysis, principal coordinate analysis (PCoA) was performed based on the Bray-Curtis distance matrix to visualize the overall structural dissimilarity of microbial communities between groups. The statistical significance of the group clustering observed in the PCoA was tested using permutational multivariate analysis of variance (PERMANOVA) with 999 permutations, implemented in the R package 'vegan' (version 2.6-4). Furthermore, to identify differentially abundant taxa across multiple taxonomic levels (from phylum to species) that were statistically significant and biologically consistent, we conducted Linear Discriminant Analysis Effect Size (LEfSe) analysis. The analysis utilized the non-parametric factorial Kruskal-Wallis sum-rank test ($\alpha = 0.05$) followed by Linear Discriminant Analysis (LDA) to estimate the effect size of each differentially abundant feature. An LDA score threshold of >2.0 was set for identifying biomarkers with meaningful biological effect.

Bacterial Culture

P. goldsteinii (BNCC356083) was cultured anaerobically in Gifu anaerobic medium (GAM, Hopebio, HB8518–1) at 37 °C. Bacterial cells were collected by centrifugation at 3200 rpm for 4 min, then resuspended in sterile PBS at a density of 5×10^8 CFU per 200 µL. Freshly prepared suspensions were used for daily oral gavage in animal experiments.

Statistical Analysis

Statistical analyses were conducted using GraphPad Prism 8 (GraphPad Software Inc, San Diego, CA, USA), unless otherwise specified. Data were presented as means ± SEM, and between-group differences were assessed using unpaired Student's *t*-test or one-way ANOVA. Correlation between microbial abundance and bone microstructure parameters was evaluated using Pearson or Spearman correlation. All statistical tests were two-tailed, and a *p*-value < 0.05 was considered statistically significant.

Results

UA Alters Bone Mass and Bone Microarchitecture in OVX Mice

To evaluate the protective effect of UA on bone mass and microstructure in OVX mice, all mice received daily oral gavage of UA (200 mg/kg) or corn oil (vehicle) for 7 weeks, beginning one week after OVX or sham surgery (Fig. 1A). The dose was selected based on previous studies demonstrating efficacy for promoting bone formation and inhibiting resorption in mice [21]. Distal femoral microstructure was evaluated by micro-CT and ABH staining. Three-dimensional (3D) reconstructions revealed that, compared to the SHAM group, the distal femoral trabeculae in the Vehicle group were thinner, fewer, and more sparsely arranged with lower overall density. UA treatment ameliorated bone loss and improved the microstructure of the bone trabeculae (Fig. 1B,D).

Trabecular bone volume fraction (BV/TV) can indirectly reflect bone volume and bone metabolism. The number of trabecular thickness (Tb.Th) and trabecular separation (Tb.Sp) were used to evaluate the spatial morphological structure of trabeculae. As shown in Fig. 1B,C, the Vehicle group had significantly decreased BMD ($p < 0.001$), trabecular BV/TV fraction ($p < 0.001$), Tb.Th ($p < 0.001$) and significantly increased Tb.Sp ($p < 0.001$) compared with the SHAM group, indicating severe bone microstructural damage and confirming successful OVX induction. Compared to the Vehicle group, UA treatment significantly improved BMD ($p < 0.01$) and trabecular microarchitecture, increasing BV/TV ($p < 0.05$) and Tb.Th ($p < 0.001$), while reducing Tb.Sp ($p < 0.01$).

UA Promotes Bone Formation and Inhibits Bone Resorption in OVX Mice

TRAP staining showed a significant increase in osteoclasts within the distal femoral medullary cavity of the Vehicle group compared to the SHAM group ($p < 0.001$), which was markedly reversed by UA administration ($p < 0.01$, Fig. 2A,B). Furthermore, immunohistochemical analysis indicated higher number of osteoblasts expressing Runx2 ($p < 0.01$), ALP ($p < 0.01$), and OCN ($p < 0.01$) in the UA group than in the Vehicle group (Fig. 2C,D). Collectively, these results demonstrate that UA exerts a bidirectional regulatory effect on bone remodeling by suppressing osteoclast-mediated resorption while enhancing osteoblast-related formation.

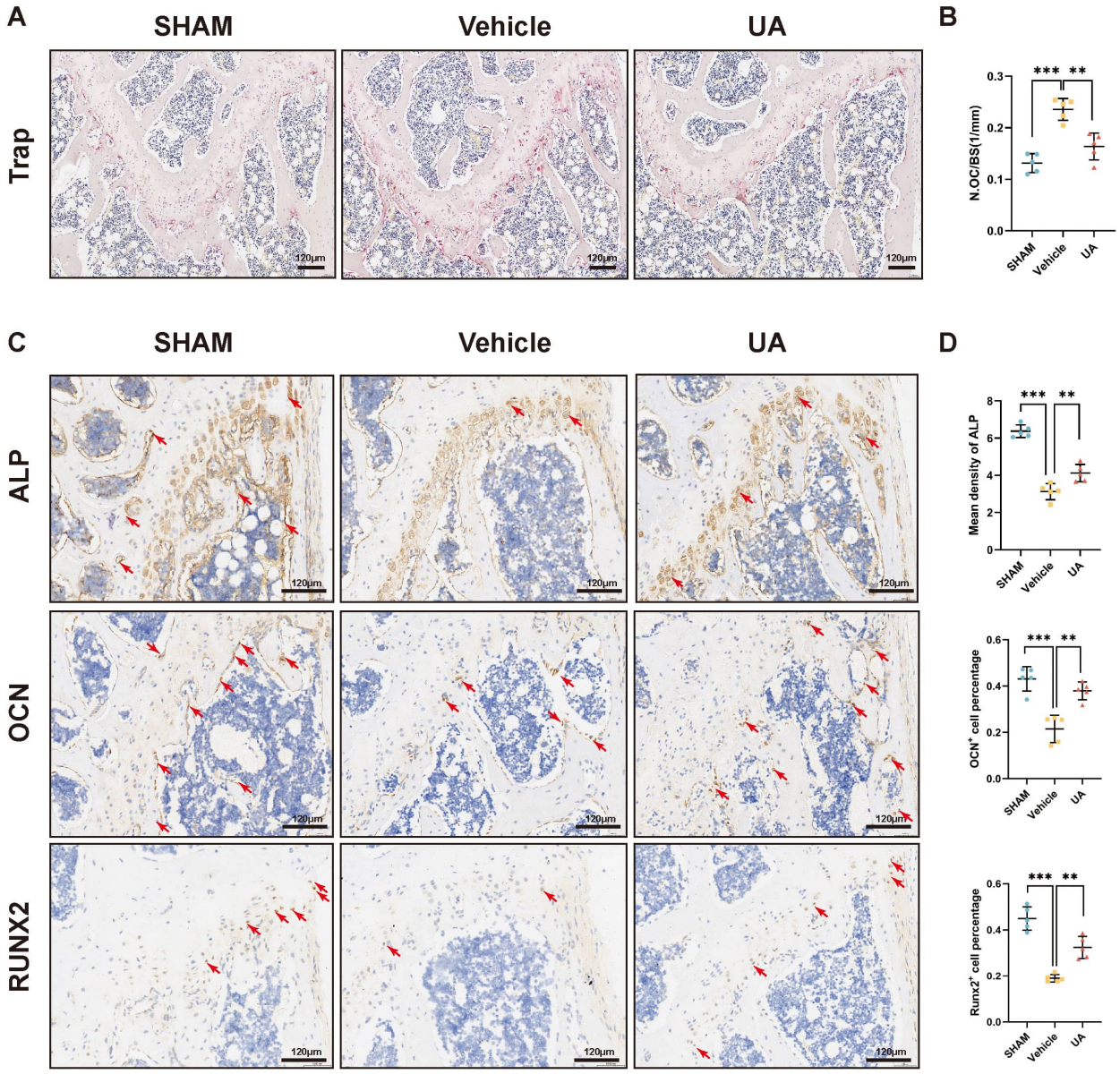

Fig. 2. UA promotes bone formation and inhibits bone resorption in OVX mice. (A,B) TRAP staining for osteoclasts on trabecular bone surfaces in the distal femur. (C,D) ALP, OCN, and RUNX2 immunohistochemical staining for labeling osteoblasts on the trabecular bone surface. Red arrows indicate positive cells. The graphs present the means ± SDs (n = 5). ***$p < 0.001$, **$p < 0.01$. TRAP, tartrate-resistant acid phosphatase; ALP, alkaline phosphatase; OCN, osteocalcin.

Transplantation of the Gut Microbial From UA-Treated Donor Ameliorates OVX-Induced Bone Loss and Destruction of the Bone Microarchitecture

To determine whether UA alleviates osteoporosis by modulating the GM, we assessed the effects of fecal microbiota transplantation (FMT) from UA-treated donor mice on bone mineral density and microstructure in recipient mice. All recipient mice received broad-spectrum antibiotics (Abx) for 1 week, followed by FMT with microbiota from donor mice gavaged with UA or corn oil for 6 weeks (Fig. 3A). Consistent with the previous findings, the distal femoral structure was evaluated using micro-CT and ABH staining, trabecular microstructure was visualized in 3D images. Compared with mice receiving vehicle-derived microbiota, recipient mice colonized with UA-derived microbiota exhibited significantly ameliorated bone loss, demonstrating thicker, more numerous, and more densely arranged trabeculae with reduced spacing (Fig. 3B,C). Quantitatively, BMD ($p < 0.001$), BV/TV ($p < 0.01$), and Tb.Th ($p < 0.01$) were substantially increased, while Tb.Sp was significantly decreased ($p < 0.001$, Fig. 3B). These findings indicate that GM transplantation from UA-treated mice ameliorates the osteoporotic phenotype.

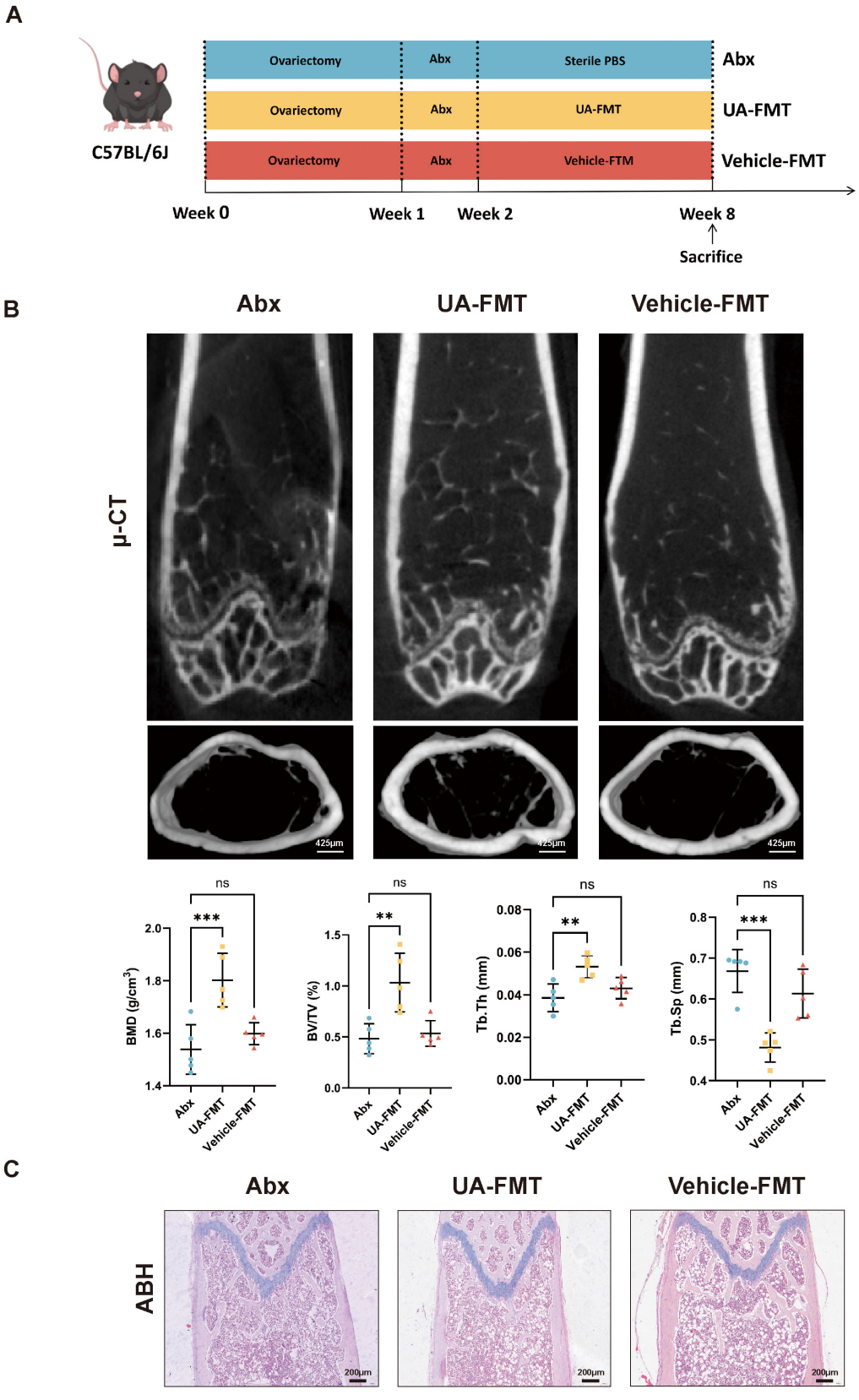

Fig. 3. Transplantation of gut microbial from UA-treated donors ameliorates OVX-induced bone loss and destruction of bone microarchitecture. (A) Recipient mice received a 1-week Abx course to deplete the gut microbiota, followed by 6 weeks of FMT from UA- or vehicle-treated donors. Bone analysis was performed at the endpoint. (B) Micro-CT results showing trabecular bone architecture in the distal femur. (C) ABH staining of the trabecular bone microarchitecture in the distal femur. The graphs present the means ± SDs (n = 5). ***$p < 0.001$, **$p < 0.01$, and ns means no significant difference.

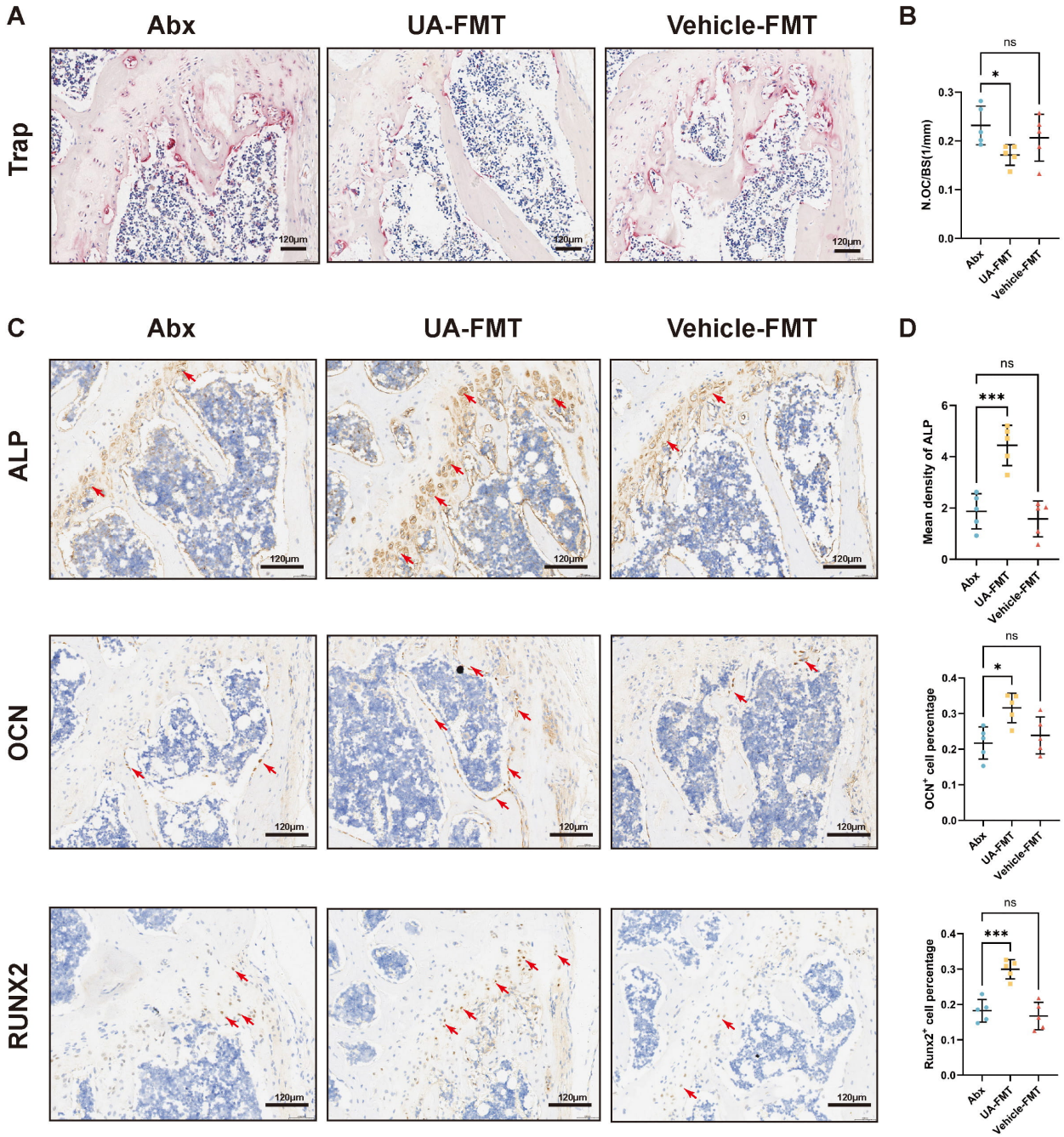

Fig. 4. Transplantation of the intestinal flora from UA-treated donor promotes bone formation and inhibits bone resorption in OVX mice. (A,B) TRAP staining for labeling osteoclasts on trabecular bone surfaces in the distal femur. (C,D) ALP, OCN, and RUNX2 immunohistochemical staining for labeling osteoblasts on the trabecular bone surface. Red arrows indicate positive cells. The graphs present the means ± SDs (n = 5). ***$p < 0.001$, *$p < 0.05$, and ns means no significant difference.

Transplantation of the Gut Microbial From UA-Treated Donor Promotes Bone Formation and Inhibits Bone Resorption in OVX Mice

Furthermore, we examined whether FMT from UA-treated donors directly affect bone formation and resorption. TRAP staining revealed fewer osteoclasts in the distal femurs of the UA-FMT group than in the Vehicle-FMT group ($p < 0.05$, Fig. 4A,B). Moreover, immunohistochemistry revealed an increased number of ALP-positive ($p < 0.001$), OCN-positive ($p < 0.05$), and Runx2-positive ($p < 0.001$) osteoblasts in the UA-FMT group (Fig. 4C,D). These results demonstrate that GM from UA-treated mice promotes bone formation and inhibits bone resorption, suggesting that the beneficial effects of UA on osteoporosis are at least partially mediated through modulation of the GM.

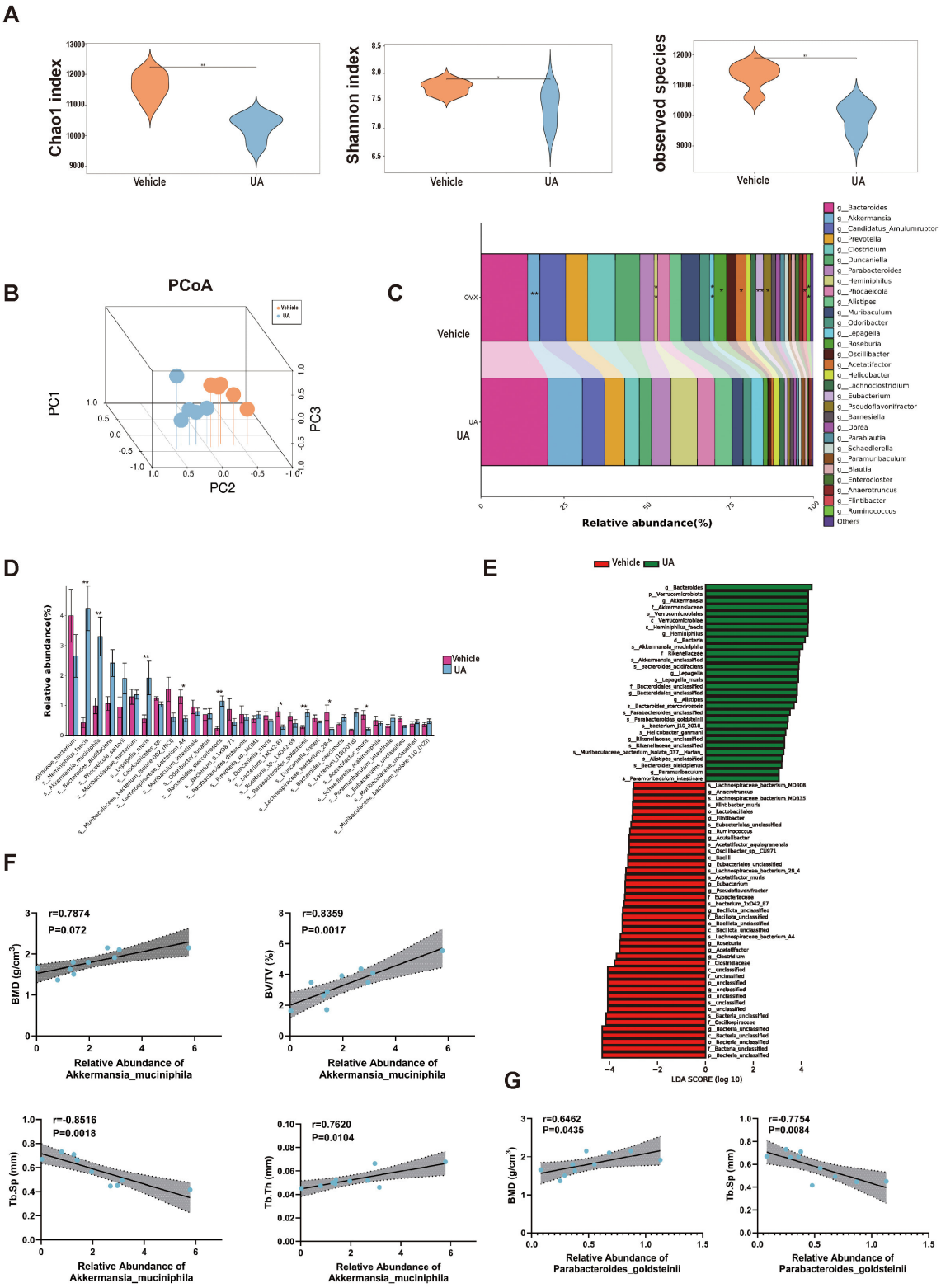

Fig. 5. Ursolic acid alters the gut microbial structure in OVX mice. (A) Alpha diversity indices (Chao1, Shannon, and observed species indices) differ significantly between the UA- and vehicle-treated groups. (B) PCoA plot of beta diversity confirming the structural divergence of the gut microbiota. (C) Species composition abundance maps at the genus level. (D) Bar chart showing the relative abundance of the top 30 microbiota at the species level in the fecal samples. (E) Linear discriminant analysis effect size (LEfSe) revealed significant differences in bacterial species abundance between the UA- and vehicle-treated groups. (F) Correlations between *A. muciniphila* and bone parameters. (G) Correlations between *P. goldsteinii* and bone parameters. The graphs present the means ± SDs ((A–E) n = 5, (F,G) n = 10). $^{**}p < 0.01$, $^{*}p < 0.05$.

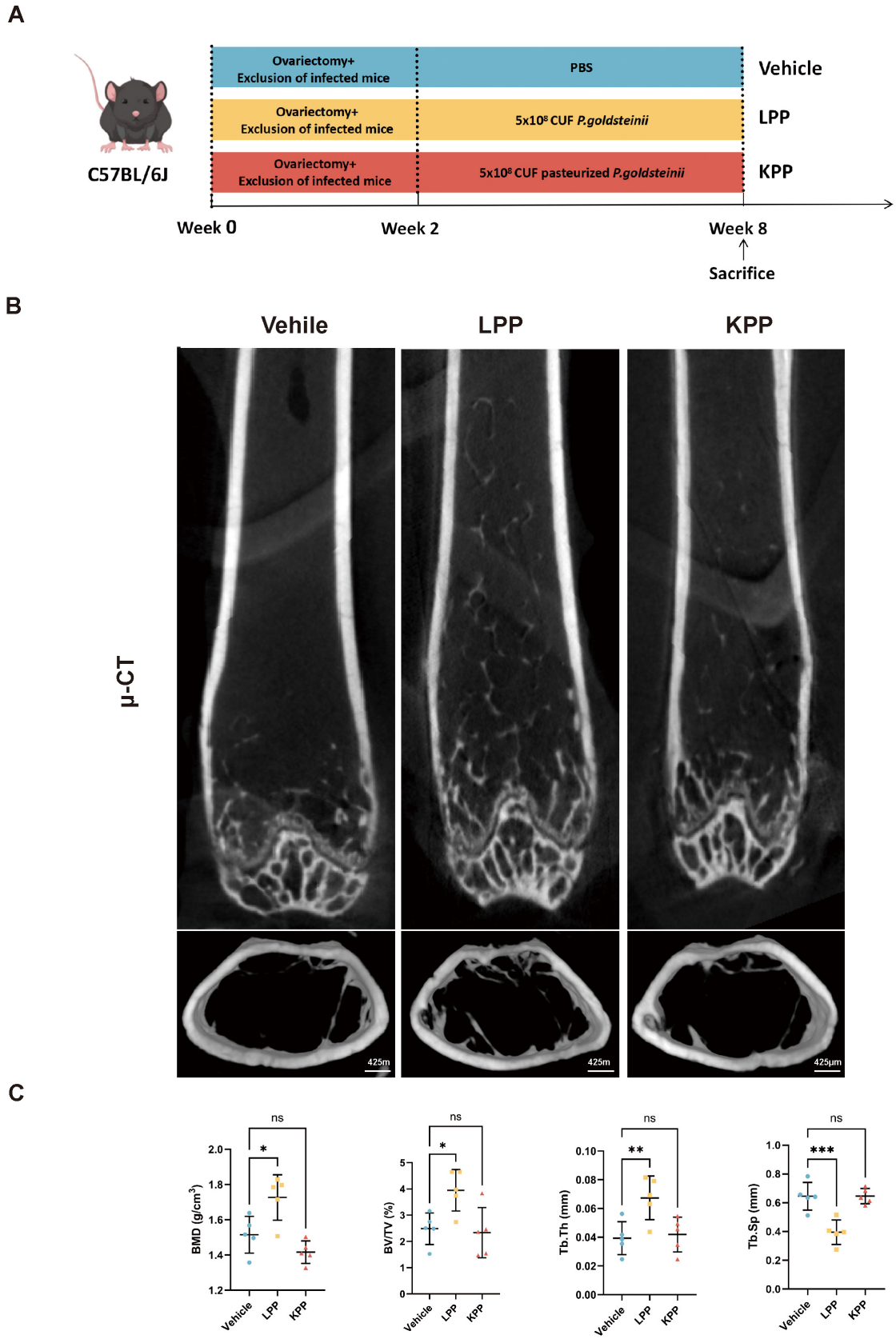

Fig. 6. LPP ameliorates OVX-induced bone loss and destruction of the bone microarchitecture. (A) OVX mice received a 6-week daily oral gavage of live *P. goldsteinii*, pasteurized *P. goldsteinii*, or PBS, followed by bone analysis at the endpoint. (B,C) Micro-CT results showing trabecular bone architecture in the distal femur. The graphs present the means ± SDs (n = 5). ***$p < 0.001$, **$p < 0.01$, *$p < 0.05$, and ns means no significant difference.

Ursolic Acid Alters the Gut Microbial Structure in OVX Mice

To identify key GM contributors to the osteoprotective effects of UA, we performed metagenomic sequencing of fecal samples from UA- and Vehicle-treated mice. The Vehicle-treated group demonstrated a significant increase in alpha diversity indices compared to the UA-treated group, as evidenced by higher Chao1 ($p < 0.01$), Shannon ($p < 0.05$), and observed species ($p < 0.01$) indices (Fig. 5A). Beta diversity analysis also revealed significant structural differences (Fig. 5B), indicating that UA alters both the diversity and intrinsic structure of the intestinal microbiota.

Specifically, at the genus level, UA gavage significantly increased the abundance of *Akkermansia* ($p < 0.01$), *Hemophilus* ($p < 0.01$), and *Lepa Gella* ($p < 0.01$). However, it decreased the abundance of *Roseburia* ($p < 0.05$), *Acetatifactor* ($p < 0.05$), *Eubacterium* ($p < 0.01$), *Pseudoflavonifractor* ($p < 0.05$), *Flintibacter* ($p < 0.05$), and *Ruminococcus* ($p < 0.01$, Fig. 5C). At the species level, UA significantly increased the abundances of *Heminiphilus_faecis* ($p < 0.01$), *Akkermansia muciniphila* (*A.muciniphila*, $p < 0.01$), *Lepagella muris* ($p < 0.01$), *Bacteroides stercorirosoris* ($p < 0.01$), *Parabacteroides goldsteinii* (*P. goldsteinii*, $p < 0.01$) while reducing the abundances of *Lachnospiraceae bacterium A4* ($p < 0.05$), *Lachnospiraceae bacterium 1xD42-87* ($p < 0.05$), *Lachnospiraceae bacterium 28-4* ($p < 0.05$), and *Acetatifactor muris* ($p < 0.05$, Fig. 5D). To identify species potentially mediating the effects of UA, we performed linear discriminant analysis of effect size (LEfSe). *Hemiphilus faecis*, *A. muciniphila*, *Bacteroides acidifaciens*, *Leptagella muris*, *Bacteroides stercorirosoris*, and *P. goldsteinii* were identified as discriminatory taxa distinguishing the UA group from the vehicle group (Fig. 5E).

We focused on *A. muciniphila* and *P. goldsteinii*. Correlation analysis revealed that *A. muciniphila* abundance was positively correlated with BV/TV ($p < 0.01$) and Tb.Th ($p < 0.05$), and significantly negatively associated with Tb.Sp ($p < 0.05$, Fig. 5F). BDM increased with higher *A. muciniphila* abundance, although this trend was not statistically significant. The *P. goldsteinii* abundance was positively correlated with the distal femur BMD ($p < 0.05$) and negatively correlated with Tb.Sp ($p < 0.01$, Fig. 5G), whereas correlations with BV/TV and Tb.Th were not significant (**Supplementary Fig. 1**).

P. goldsteinii Alleviates Bone Mass and Bone Microarchitecture in OVX Mice

To evaluate the effects of *P. goldsteinii* on bone loss, OVX mice received daily oral gavage for 6 weeks with vehicle (PBS), live *P. goldsteinii* (LPP), or pasteurized *P. goldsteinii* (KPP) (Fig. 6A). Importantly, supplementation with live, but not pasteurized, *P. goldsteinii* significantly increased distal femoral BMD ($p < 0.05$), BV/TV ($p < 0.05$), and Tb.Th ($p < 0.01$), while decreasing Tb.Sp ($p < 0.001$) in OVX mice, thereby improving the microstructure of the bone trabeculae (Fig. 6B,C). These results suggest that the bone-protective effects may depend on bioactive metabolites produced by *P. goldsteinii*.

Discussion

Despite increasing interest in the GM in osteoporosis, the specific contribution of individual bacterial species on bone metabolism and the identification of novel probiotics that both improve bone mass and effectively colonize the host remain unresolved challenges. UA is a natural constituents of many herbal extracts [15]. Over the past decade, UA has demonstrated a range of pharmacological activities, including anti-osteoporotic effects. However, whether the GM contributes to these beneficial effects remains entirely unexplored.

Our study revealed that UA treatment effectively ameliorates bone loss and improves trabecular microarchitecture in OVX mice. More importantly, employing FMT, we observed that the osteoprotective effects of UA are transferable via the GM: recipient mice receiving microbiota from UA-treated donors recapitulated the improvements in bone mass and the reduction in bone resorption. These observations demonstrate that GM remodeling is a key mechanism underlying UA's anti-osteoporosis. While previous studies have indicated that UA ameliorates conditions such as sarcopenia [22] or neuropathic pain [23] via GM modulation, to our knowledge, this is the first evidence linking UA-mediated improvement of osteoporosis to GM modulation.

Compared with 16S rRNA gene amplicon sequencing, metagenomic sequencing provides higher taxonomic resolution, enabling species- or strain-level identification [24], which is crucial for detecting key microbial contributors to bone metabolism. Our metagenomic analysis revealed significant alteration in the structure of the GM in OVX mice after UA treatment. Notably, UA treatment decreased alpha diversity compared with controls, a finding that aligns with previous evidence but also contrasts with others [25]. This reduction is likely due to OVX-induced estrogen deficiency impairing the intestinal environment and the potential direct antimicrobial effects of UA on certain species [26].

Importantly, UA induced significant shifts in specific taxa, most prominently enriching *Akkermansia* (particularly *A. muciniphila*) and *P. goldsteinii*. *A. muciniphila*, recognized as a promising next-generation probiotic, has been directly associated with skeletal health [27]. Evidence demonstrates that extracellular vesicles derived from *A. muciniphila* localize in bone, enhance osteogenesis, and suppress osteoclastogenesis, thereby attenuating OVX-induced osteoporosis [13]. These previous reports align with our observation that *A. muciniphila* abundance correlates positively with BMD, BV/TV, and Tb.Th, and negatively with Tb.Sp.

The significant enrichment of *P. goldsteinii* by UA represents a novel observation in the context of osteoporosis. Although direct links between *P. goldsteinii* and bone metabolism have not been established, its documented biological activities suggest plausible mechanisms. *P. goldsteinii* possesses anti-inflammatory effects, partly because its lipopolysaccharide (LPS) antagonizes TLR4 signaling and ameliorates conditions such as COPD [28]. Furthermore, it improves intestinal barrier integrity and reduces obesity in high-fat diet models [29]. Critically, both TLR4 inhibition and intestinal barrier repair have been demonstrated to ameliorate osteoporosis progression [12,30]. Therefore, we hypothesize that *P. goldsteinii* contributes to the osteoprotective effects of UA by dampening systemic inflammation via TLR4 modulation and/or by enhancing intestinal barrier integrity.

LEfSe analysis identified *Akkermansia muciniphila* and *P. goldsteinii* as discriminative taxa in UA-treated GM. Correlation analysis further linked *A. muciniphila* with improved bone metrics. While *P. goldsteinii* abundance was positively associated with BMD and negatively with Tb.Sp, correlations with BV/TV and Tb.Th were not significant, likely reflecting limited sample size and statistical power. Hence, larger studies are warranted to validate these associations.

To further investigate the impact of *P. goldsteinii* on bone mass, OVX mice were administered either live *P. goldsteinii*, pasteurized *P. goldsteinii*, or PBS via oral gavage daily for two months. Micro-CT analysis revealed that only live *P. goldsteinii* significantly ameliorated bone loss and preserved bone microarchitecture in OVX mice, suggesting that its osteoprotective effects are likely mediated by metabolites produced by viable bacterial cells.

A limitation of this study is that the specific metabolite(s) derived from *P. goldsteinii* responsible for the anti-osteoporotic effects remain unidentified. To address this, in our subsequent studies, we plan to perform untargeted metabolomic sequencing on bone marrow flushes, fecal samples, and supernatants from both cultured and uncultured *P. goldsteinii* obtained from *P. goldsteinii*-colonized OVX mice. The objective is to identify metabolites showing significant abundance differences across all three sample types. The impact of these candidate metabolites on bone mass will then be defined through a structured series of *in vivo* and *in vitro* experiments.

Conclusion

In conclusion, ursolic acid ameliorates osteoporosis by modulating the gut microbiota. The underlying mechanism is likely mediated by an increased abundance of the probiotic *Akkermansia muciniphila*. Furthermore, this study identified *P. goldsteinii* as a potential probiotic candidate for osteoporosis, providing a groundwork for future mechanistic investigations and translational research.

Availability of Data and Materials

All source data generated in this work reside in the article and supplementary materials, and further inquiries can be directed to the corresponding authors.

Author Contributions

YY and LJ designed the research study. MW and YY performed the research. ZB, JW and XL provided help and advice on the micro-CT experiments. BZ, GS and LC analyzed the data. LJ drafted the manuscript. All authors contributed to critical revision of the manuscript for important intellectual content. All authors read and approved the final manuscript. All authors have participated sufficiently in the work and agreed to be accountable for all aspects of the work.

Ethics Approval and Consent to Participate

All animal experiments were performed in adherence to the approved protocols in Zhejiang University of Traditional Chinese Medicine Animal Ethics Committee (ID: 20250217-28), relevant institutional policies, and national standards for laboratory animal welfare.

Acknowledgment

We gratefully acknowledge the technical support from the Medical Research Center Public Platform at Zhejiang Chinese Medical University.

Funding

This study was supported by the Research and Development Program for ‘Pioneer’ and ‘Leading Goose’ of Zhejiang Province (2024C03213), the Science and Technology Innovation Activity Plan for College Students in Zhejiang Province in 2024 (2024R410B059), the Research Project of Zhejiang Chinese Medical University (2023JKZKTS41) and the Science and Technology Plan of TCM of Zhejiang Province (2024ZL514).

Conflict of Interest

The authors declare no conflict of interest.

Supplementary Material

Supplementary material associated with this article can be found, in the online version, at https://doi.org/10.24976/Discov.Med.202537203.250.

References

[1] Compston JE, McClung MR, Leslie WD. Osteoporosis. Lancet. 2019; 393: 364–376. https://doi.org/10.1016/S0140-6736(18)32112-3.

[2] Kirkham-Wilson F, Dennison E. Osteoporosis and Rheumatoid Arthritis: A Review of Current Understanding and Practice.

British Journal of Hospital Medicine . 2024; 85: 1–11. https://doi.org/10.12968/hmed.2024.0341.

[3] Mohammadi SM, Moniri S, Mohammadhoseini P, Hanafi MG, Farasat M, Cheki M. A Computed Tomography-based Radiomics Analysis of Low-energy Proximal Femur Fractures in the Elderly Patients. Current Radiopharmaceuticals. 2023; 16: 222–232. https://doi.org/10.2174/1874471016666230321120941.

[4] Salari N, Darvishi N, Bartina Y, Larti M, Kiaei A, Hemmati M, *et al*. Global prevalence of osteoporosis among the world older adults: a comprehensive systematic review and meta-analysis. Journal of Orthopaedic Surgery and Research. 2021; 16: 669. https://doi.org/10.1186/s13018-021-02821-8.

[5] Zheng XQ, Wang DB, Jiang YR, Song CL. Gut microbiota and microbial metabolites for osteoporosis. Gut Microbes. 2025; 17: 2437247. https://doi.org/10.1080/19490976.2024.2437247.

[6] Yang Y, Hao C, Jiao T, Yang Z, Li H, Zhang Y, *et al*. Osteoarthritis treatment via the GLP-1-mediated gut-joint axis targets intestinal FXR signaling. Science. 2025; 388: eadt0548. https://doi.org/10.1126/science.adt0548.

[7] Wang D, Cai J, Pei Q, Yan Z, Zhu F, Zhao Z, *et al*. Gut microbial alterations in arginine metabolism determine bone mechanical adaptation. Cell Metabolism. 2024; 36: 1252–1268.e8. https://doi.org/10.1016/j.cmet.2024.04.004.

[8] Li JY, Chassaing B, Tyagi AM, Vaccaro C, Luo T, Adams J, *et al*. Sex steroid deficiency-associated bone loss is microbiota dependent and prevented by probiotics. The Journal of Clinical Investigation. 2016; 126: 2049–2063. https://doi.org/10.1172/JCI86062.

[9] Zhang YW, Cao MM, Li YJ, Lu PP, Dai GC, Zhang M, *et al*. Fecal microbiota transplantation ameliorates bone loss in mice with ovariectomy-induced osteoporosis via modulating gut microbiota and metabolic function. Journal of Orthopaedic Translation. 2022; 37: 46–60. https://doi.org/10.1016/j.jot.2022.08.003.

[10] Guo M, Liu H, Yu Y, Zhu X, Xie H, Wei C, *et al*. *Lactobacillus rhamnosus* GG ameliorates osteoporosis in ovariectomized rats by regulating the Th17/Treg balance and gut microbiota structure. Gut Microbes. 2023; 15: 2190304. https://doi.org/10.1080/19490976.2023.2190304.

[11] Li B, Liu M, Wang Y, Gong S, Yao W, Li W, *et al*. Puerarin improves the bone micro-environment to inhibit OVX-induced osteoporosis via modulating SCFAs released by the gut microbiota and repairing intestinal mucosal integrity. Biomedicine & Pharmacotherapy. 2020; 132: 110923. https://doi.org/10.1016/j.biopha.2020.110923.

[12] Chen C, Cao Z, Lei H, Zhang C, Wu M, Huang S, *et al*. Microbial Tryptophan Metabolites Ameliorate Ovariectomy-Induced Bone Loss by Repairing Intestinal AhR-Mediated Gut-Bone Signaling Pathway. Advanced Science. 2024; 11: e2404545. https://doi.org/10.1002/advs.202404545.

[13] Liu JH, Chen CY, Liu ZZ, Luo ZW, Rao SS, Jin L, *et al*. Extracellular Vesicles from Child Gut Microbiota Enter into Bone to Preserve Bone Mass and Strength. Advanced Science. 2021; 8: 2004831. https://doi.org/10.1002/advs.202004831.

[14] Lyu Z, Hu Y, Guo Y, Liu D. Modulation of bone remodeling by the gut microbiota: a new therapy for osteoporosis. Bone Research. 2023; 11: 31. https://doi.org/10.1038/s41413-023-00264-x.

[15] Woźniak Ł, Skąpska S, Marszałek K. Ursolic Acid–A Pentacyclic Triterpenoid with a Wide Spectrum of Pharmacological Activities. Molecules. 2015; 20: 20614–20641. https://doi.org/10.3390/molecules201119721.

[16] Cheng M, Liang XH, Wang QW, Deng YT, Zhao ZX, Liu XY. Ursolic Acid Prevents Retinoic Acid-Induced Bone Loss in Rats. Chinese Journal of Integrative Medicine. 2019; 25: 210–215. https://doi.org/10.1007/s11655-018-3050-y.

[17] Zheng H, Feng H, Zhang W, Han Y, Zhao W. Targeting autophagy by natural product Ursolic acid for prevention and treatment of osteoporosis. Toxicology and Applied Pharmacology. 2020; 409: 115271. https://doi.org/10.1016/j.taap.2020.115271.

[18] Lee SU, Park SJ, Kwak HB, Oh J, Min YK, Kim SH. Anabolic activity of ursolic acid in bone: Stimulating osteoblast differentiation in vitro and inducing new bone formation in vivo. Pharmacological Research. 2008; 58: 290–296. https://doi.org/10.1016/j.phrs.2008.08.008.

[19] Tian C, Li J, Bao Y, Gao L, Song L, Li K, *et al*. Ursolic acid ameliorates obesity of mice fed with high-fat diet via alteration of gut microbiota and amino acid metabolism. Frontiers in Microbiology. 2023; 14: 1183598. https://doi.org/10.3389/fmicb.2023.1183598.

[20] Jing D, Li F, Jiang M, Cai J, Wu Y, Xie K, *et al*. Pulsed electromagnetic fields improve bone microstructure and strength in ovariectomized rats through a Wnt/Lrp5/β-catenin signaling-associated mechanism. PLoS ONE. 2013; 8: e79377. https://doi.org/10.1371/journal.pone.0079377.

[21] Yu SG, Zhang CJ, Xu XE, Sun JH, Zhang L, Yu PF. Ursolic acid derivative ameliorates streptozotocin-induced diabestic bone deleterious effects in mice. International Journal of Clinical and Experimental Pathology. 2015; 8: 3681–3690.

[22] She M, Li T, Zhou L, Deng Z, Huang M, Yan Y, *et al*. Ursolic acid attenuates sarcopenia through IL-17a-related gut-muscle axis in senile diabetic mice and myotube model. The Journal of Nutritional Biochemistry. 2025; 143: 109940. https://doi.org/10.1016/j.jnutbio.2025.109940.

[23] Rong ZJ, Chen M, Cai HH, Liu GH, Chen JB, Wang H, *et al*. Ursolic acid molecules dock MAPK1 to modulate gut microbiota diversity to reduce neuropathic pain. Neuropharmacology. 2024; 252: 109939. https://doi.org/10.1016/j.neuropharm.2024.109939.

[24] Rausch P, Rühlemann M, Hermes BM, Doms S, Dagan T, Dierking K, *et al*. Comparative analysis of amplicon and metagenomic sequencing methods reveals key features in the evolution of animal metaorganisms. Microbiome. 2019; 7: 133. https://doi.org/10.1186/s40168-019-0743-1.

[25] Sheng Q, Li F, Chen G, Li J, Li J, Wang Y, *et al*. Ursolic Acid Regulates Intestinal Microbiota and Inflammatory Cell Infiltration to Prevent Ulcerative Colitis. Journal of Immunology Research. 2021; 2021: 6679316. https://doi.org/10.1155/2021/6679316.

[26] Wang CM, Jhan YL, Tsai SJ, Chou CH. The Pleiotropic Antibacterial Mechanisms of Ursolic Acid against Methicillin-Resistant Staphylococcus aureus (MRSA). Molecules. 2016; 21: 884. https://doi.org/10.3390/molecules21070884.

[27] Rodrigues VF, Elias-Oliveira J, Pereira ÍS, Pereira JA, Barbosa SC, Machado MSG, *et al*. *Akkermansia muciniphila* and Gut Immune System: A Good Friendship That Attenuates Inflammatory Bowel Disease, Obesity, and Diabetes. Frontiers in Immunology. 2022; 13: 934695. https://doi.org/10.3389/fimmu.2022.934695.

[28] Lai HC, Lin TL, Chen TW, Kuo YL, Chang CJ, Wu TR, *et al*. Gut microbiota modulates COPD pathogenesis: role of anti-inflammatory *Parabacteroides goldsteinii* lipopolysaccharide. Gut. 2022; 71: 309–321. https://doi.org/10.1136/gutjnl-2020-322599.

[29] Wu TR, Lin CS, Chang CJ, Lin TL, Martel J, Ko YF, *et al*. Gut commensal *Parabacteroides goldsteinii* plays a predominant role in the anti-obesity effects of polysaccharides isolated from *Hirsutella sinensis*. Gut. 2019; 68: 248–262. https://doi.org/10.1136/gutjnl-2017-315458.

[30] Park S, Yoon K, Hong E, Kim MW, Kang MG, Mizuno S, *et al*. Tm4sf19 inhibition ameliorates inflammation and bone destruction in collagen-induced arthritis by suppressing TLR4-mediated inflammatory signaling and abnormal osteoclast activation. Bone Research. 2025; 13: 40. https://doi.org/10.1038/s41413-025-00419-y.